SCIENCE CHINA
Information Sciences

• RESEARCH PAPER •

August 2026, Vol. 69, Iss. 8, 182205:1–182205:15
https://doi.org/10.1007/s11432-025-4897-9

Prescribed performance-based fixed-time control of nonlinear systems with application to flight dynamics

Yingxin SHOU[1], Bin XU[2*], Yongping PAN[1] & Hai WANG[3]

[1]School of Automation, Southeast University, Nanjing 210096, China
[2]School of Automation, Northwestern Polytechnical University, Xi'an 710072, China
[3]Discipline of Engineering and Energy, Centre of Water, Energy, and Waste, Murdoch University, Perth WA 6150, Australia

Received 18 April 2025/Revised 30 June 2025/Accepted 25 July 2025/Published online 8 July 2026

Abstract This study presents a robust adaptive controller for strict-feedback nonlinear systems with dynamic uncertainties and external disturbances, aiming to achieve fixed-time convergence under prescribed performance constraints. The proposed approach employs fuzzy logic systems integrated with robust integral terms based on error signs for the effective estimation of uncertainties and disturbances. Using these estimates, a parallel identification system is constructed to maintain dynamic consistency with the original system dynamics. By embedding prescribed performance functions, the designed controller explicitly enforces transient constraints and ensures fixed-time convergence of tracking errors, independent of the initial states. Stability analysis rigorously demonstrates semi-global convergence of the identification errors and fixed-time convergence of the tracking errors. The simulation results verify the effectiveness and superior disturbance-rejection and tracking performance of the proposed scheme.

Keywords nonlinear system, robust integral of the sign of the error, parallel identification system, fixed-time convergence, state constraint control

Citation Shou Y X, Xu B, Pan Y P, et al. Prescribed performance-based fixed-time control of nonlinear systems with application to flight dynamics. Sci China Inf Sci, 2026, 69(8): 182205, https://doi.org/10.1007/s11432-025-4897-9

1 Introduction

Nonlinear characteristics and phenomena are ubiquitous in both nature and engineering, including in circuits, robotics, aircraft, and other complex systems. The inherent uncertainty in nonlinear phenomena, combined with the requirement for high-precision control, renders the design of control algorithms based on mathematical theory increasingly complex. However, most mature control theories rely on known models, which limits the generalization of nonlinear control. For instance, the dynamics of aircraft in complex environments are characterized by strong nonlinearity and coupling, making it difficult to develop accurate models of aircraft dynamics. This leads to significant uncertainties in the structure and parameters of the models. To effectively reduce the dependency of control systems on models, techniques such as parameter identification, robust control [1, 2], active disturbance-rejection control [3, 4], and adaptive control [5–7] have been widely employed.

Two primary approaches have been proposed for handling the impact of unknowns and uncertainties in the model on the control system: the first is enhancing the robustness to accommodate the impact of unknowns, and the second involves compensating for the uncertainty. The former is represented by sliding-mode control having a variable-structure property, which ensures that the state of the system follows a desired sliding-mode trajectory that is unaffected by internal state perturbations or external disturbances. Ref. [8] proposed a composite disturbance filter as a means of compensating for disturbances and attenuation errors. Moreover, a sliding-mode disturbance observer was designed [9] to ensure finite-time convergence even in the presence of strong disturbances. Fixed-time control methods [10] address the dependency of the convergence time on the initial conditions by setting the control parameters. This approach guarantees an upper bound on the convergence time as well as a faster convergence speed. The prescribed-time control method [11, 12] employs adjustable control parameters to ensure that the convergence time of the system does not exceed a pre-specified time parameter. However, sliding-mode control is inherently a discontinuous control strategy, leading to chattering and high-frequency switching behaviors. The robust integral of the sign of the error (RISE) control technique [13–15] employs high-gain proportional terms,

* Corresponding author (email: smileface.binxu@gmail.com)

integral state feedback, and integral error terms in an estimator to compensate for time-varying disturbances while avoiding the use of higher-order derivatives of the states and discontinuous functions of the system. Nevertheless, RISE requires substantial control energy and is thus difficult to implement in practical systems with actuator limitations.

Another representative uncertainty-control theory is intelligent control, which leverages the function approximation capabilities of methods such as neural networks [16, 17], fuzzy logic systems (FLS) [18–20], support vector machines [21, 22], and generalized learning techniques [23–25]. These methods, in combination with data analysis techniques, are used to model the nonlinear relationship between the inputs and states of a system, mitigating the impact of unmodeled dynamics on the control performance. The use of FLS to accurately learn the dynamics of aircraft is demonstrated in [26–28]. The obtained results were fed forward into backstepping control laws to achieve high-precision flight control. However, most intelligent control techniques [29–31] rely on Lyapunov stability as the control objective. When the system meets the external tracking objectives, learning ceases as the tracking error converges, potentially leaving some model uncertainties unlearned. Composite learning-control techniques introduce learning quality evaluation metrics into the learning update laws through indirect signals, thus circumventing issues related to the quantification of unknown uncertainties. One approach involves filtering the inputs to the system and predicting the difference between the predicted and current inputs to construct the learning errors [32]. In another approach, historical data regarding the state of the system are collected, and interval excitation principles and definite integral statistical techniques are used to reveal inherent invariant state properties as evaluation metrics for intelligent learning [33, 34]. A third approach establishes parallel nonlinear estimation models and uses the differences between the estimated and actual states as the learning evaluation metrics [35, 36]. Intelligent control methods address regular uncertainties but face inefficiencies in dealing with unforeseen disturbances commonly encountered in nonlinear systems. Additionally, the learning techniques themselves often introduce reconstruction residuals, limiting the ability of the control system to achieve uniformly bounded tracking.

Considering the above analysis, this study combines the precise feedforward effect of composite learning with the high-gain feedback effect of RISE for achieving robust adaptive control under state prediction. This approach aims to improve both the transient and steady-state performance of control systems subject to dynamic uncertainties and irregular disturbances. The contributions of this study are summarized as follows.

(1) A parallel identification system employing FLS combined with RISE techniques is proposed for the accurate estimation of dynamic uncertainties and external disturbances, where the "quality of estimation" is indirectly assessed using state-estimation errors as metrics.

(2) The designed fixed-time backstepping control strategy integrated with a fixed-time filter incorporates prescribed performance control to ensure precise convergence of the tracking errors within a predefined fixed-time interval, while simultaneously guaranteeing explicit constraints on the states of the system.

(3) The controller accurately learns the uncertainty through indirect evaluation, unifies the indirect estimation, fixed-time convergence, and prescribed performance, and enhances the robust adaptive control capability.

The remainder of this paper is organized as follows. Section 2 presents an introduction to the model of the system dynamics and some necessary preliminary work. Section 3 presents the design of an identification model and the constraint controller. The stability of the system is analyzed in Section 4. The simulation results are discussed in Section 5 to validate the effectiveness of the proposed approach. Finally, the conclusion is drawn in Section 6.

2 System dynamics and formulation

2.1 Dynamics model

The n-th order strict-feedback nonlinear system with uncertainty and disturbance is represented as

$$\begin{cases} \dot{\upsilon}_1 = f_1\left(\bar{\upsilon}_1\right) + g_1 \upsilon_2 + d_1, \\ \dot{\upsilon}_i = f_i\left(\bar{\upsilon}_i\right) + g_i \upsilon_{i+1} + d_i, \quad i = 2, \cdots, n-1, \\ \dot{\upsilon}_n = f_n\left(\bar{\upsilon}_n\right) + g_n \mu + d_n, \end{cases} \tag{1}$$

where υ_i represents the states of the system, μ is the input to the system, $f_i\left(\bar{\upsilon}_i\right)$ is the dynamic uncertainty, where $\bar{\upsilon}_i = \left[\upsilon_1, \cdots, \upsilon_i\right]^{\mathrm{T}}$, g_i is the known control-gain function, d_i is the external disturbance, and $i = 1, \cdots, n$, n is the system order.

To achieve the required accuracy level $\varepsilon_i \in \Re$, FLS [37] can be utilized to approximate the uncertainty function

$f_i(\bar{\upsilon}_i)$ of the system using a compact set Ω_{υ_i}. The following linear combination is obtained:

$$\sup_{\upsilon_i \in \Omega_{\upsilon_i}} \left| f_i(\bar{\upsilon}_i) - \hat{\sigma}_i^{\mathrm{T}} \varphi_i(\bar{\upsilon}_i) \right| \leqslant \varepsilon_i, \tag{2}$$

where $\hat{\sigma}_i \in \Re^{\iota_i \times 1}$ is the adaptive fuzzy weight. $\varphi_i(\bar{\upsilon}_i) = [\varphi_{i,1}(\bar{\upsilon}_i), \varphi_{i,2}(\bar{\upsilon}_i), \cdots, \varphi_{i,\iota_i}(\bar{\upsilon}_i)]^{\mathrm{T}} \in \Re^{\iota_i \times 1}$ is the basis function in the "If-Then" rule as follows:

$$\begin{gathered}
\varphi_{i,j}(\bar{\upsilon}_i) = \frac{W_{F_{i,j}}(\bar{\upsilon}_i)}{\sum_{j=1}^{\iota_i} W_{F_{i,j}}(\bar{\upsilon}_i)}, \\
W_{F_{i,j}}(\bar{\upsilon}_i) = \frac{1}{\sqrt{2\pi}\varrho_{i,j}} \exp\left[-\frac{\|\bar{\upsilon}_i - \mathrm{X}_{i,j}\|^2}{2\varrho_{i,j}^2}\right],
\end{gathered} \tag{3}$$

where ι_i is the number of fuzzy rules, $\varrho_{i,j}$ is the width vector, $X_{i,j} = [x_{1,j}, \cdots, x_{i,j}]^{\mathrm{T}} \in \Re^{i \times 1}$ is the center of the fuzzy sets. Furthermore, the optimal fuzzy weight is represented as

$$\begin{gathered}
f_i(\bar{\upsilon}_i) = \sigma_i^{*\mathrm{T}} \varphi_i(\bar{\upsilon}_i) + \varepsilon_i, \\
\sigma_i^* = \arg \min_{\hat{\sigma}_i \in \Omega_{\hat{\sigma}_i}} \left\{ \sup_{\upsilon_i \in \Omega_{\upsilon_i}} \left| f_i(\bar{\upsilon}_i) - \hat{\sigma}_i^{\mathrm{T}} \varphi_i(\bar{\upsilon}_i) \right| \right\}.
\end{gathered} \tag{4}$$

Remark 1. The derivative of the basis function $\dot{\varphi}_i(\bar{\upsilon}_i) = [\dot{\varphi}_{i,1}(\bar{\upsilon}_i), \dot{\varphi}_{i,2}(\bar{\upsilon}_i), \cdots, \dot{\varphi}_{i,\iota_i}(\bar{\upsilon}_i)]^{\mathrm{T}} \in \Re^{\iota_i \times 1}$, where $\dot{\varphi}_{i,j}(\bar{\upsilon}_i)$ is calculated as

$$\begin{gathered}
\dot{\varphi}_{i,j}(\bar{\upsilon}_i) = -\frac{\sum_{j=1}^{\iota_i} \dot{W}_{F_{i,j}}(\bar{\upsilon}_i) W_{F_{i,j}}(\bar{\upsilon}_i)}{\left[\sum_{j=1}^{\iota_i} W_{F_{i,j}}(\bar{\upsilon}_i)\right]^2} + \frac{\dot{W}_{F_{i,j}}(\bar{\upsilon}_i)}{\sum_{j=1}^{\iota_i} W_{F_{i,j}}(\bar{\upsilon}_i)}, \\
\dot{W}_{F_{i,j}}(\bar{\upsilon}_i) = -\sum_{k=1}^{i} \frac{|\upsilon_k - \mathrm{x}_{k,j}|}{\sqrt{2\pi}\varrho_{i,j}^3} \exp\left[-\frac{\|\bar{\upsilon}_i - \mathrm{X}_{i,j}\|^2}{2\varrho_{i,j}^2}\right] \dot{\upsilon}_k.
\end{gathered} \tag{5}$$

Thus, the derivatives can be rewritten as $\dot{\varphi}_{i,j}(\bar{\upsilon}_i) = \sum_{k=1}^{i} \varphi'_{i,j,k}(\bar{\upsilon}_i)\dot{\upsilon}_k$.

Assumption 1 ([32])**.** The control-gain function g_i is a bounded function satisfying $|g_i| \leqslant \bar{g}_i$ and $\bar{g}_i > 0$. The disturbance d_i is second-order differentiable with $d_i \in L_\infty$, $\dot{d}_i \in L_\infty$, and $\ddot{d}_i \in L_\infty$.

Assumption 2 ([38])**.** The optimal weight σ_i^* is bounded by $\|\sigma_i^*\|_F \leqslant \bar{\sigma}_i$; the function $\varphi_i(\bar{\upsilon}_i)$ and the error ε_i are second-order differentiable and are bounded by a known bound.

2.2 Control goal

The control goal is to design a fixed-time constraint controller with an identification model to drive the state υ_1 of the uncertain nonlinear strict-feedback system to track the desired command υ_1^r, while satisfying the state constraints. The control scheme is shown in Figure 1.

3 Controller design

Step 1: Considering the identification of uncertainty $f_1(\bar{\upsilon}_1)$ and disturbance d_1, the serial-parallel identification system (SPIS) is constructed as

$$\dot{\hat{\upsilon}}_1 = \hat{\sigma}_1^{\mathrm{T}} \varphi_1(\bar{\hat{\upsilon}}_1) + g_1 \hat{\upsilon}_2 + \delta_1, \tag{6}$$

where $\hat{\upsilon}_1$ represents the identified state and δ_1 is the RISE feedback term defined by (7).

If the identification error and the filtered identification error are defined as $\tilde{\upsilon}_1 = \upsilon_1 - \hat{\upsilon}_1$ and $s_1 = \dot{\tilde{\upsilon}}_1 + \alpha_1 \tilde{\upsilon}_1$, respectively, the proposed term δ_1 is represented as

$$\delta_1 = k_1 \tilde{\upsilon}_1 - k_1 \tilde{\upsilon}_1(0) + \chi_1, \tag{7}$$

where the auxiliary signal χ_1 is obtained from the following differential equation:

$$\dot{\chi}_1 = (k_1 \alpha_1 + \gamma_1) \tilde{\upsilon}_1 + \beta_1 \mathrm{sign}(\tilde{\upsilon}_1) + \dot{g}_1 \tilde{\upsilon}_2 - g_1 \alpha_2 \tilde{\upsilon}_2. \tag{8}$$

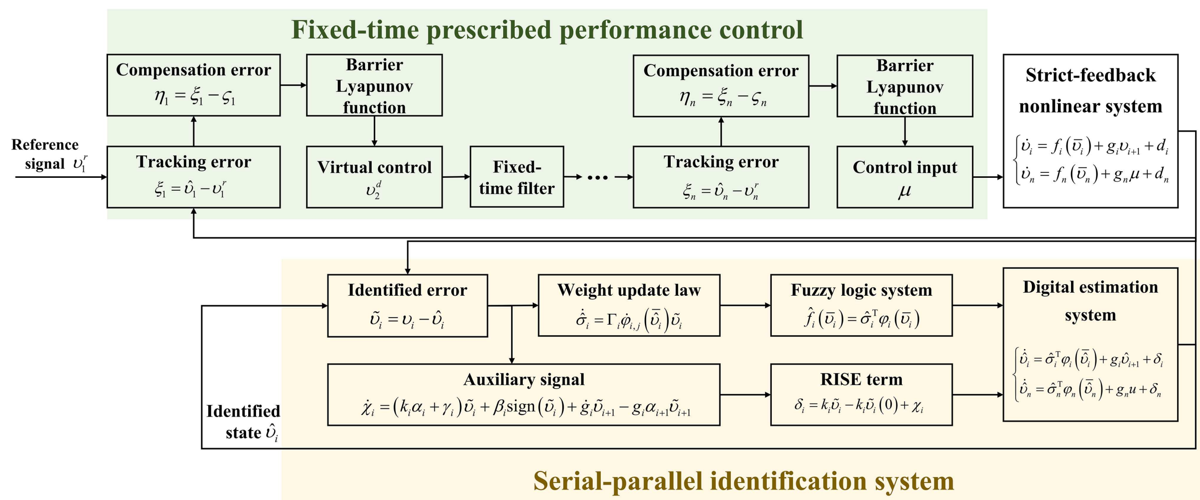

Figure 1 (Color online) Control scheme.

Here $k_1 > 0$, $\alpha_1 > 0$, $\gamma_1 > 0$, $\beta_1 > 0$, and $\alpha_2 > 0$ are the positive design parameters; $\tilde{\upsilon}_2 = \upsilon_2 - \hat{\upsilon}_2$ is the identification error; and $\hat{\upsilon}_2$ is the identified state obtained from (16).

The law for updating the fuzzy weight is expressed as

$$\dot{\hat{\sigma}}_1 = \Gamma_1 \dot{\varphi}_1 \left(\bar{\hat{\upsilon}}_1\right) \tilde{\upsilon}_1, \tag{9}$$

where $\dot{\varphi}_1 \left(\bar{\hat{\upsilon}}_1\right) = \dot{\varphi}_{1,1} \left(\bar{\hat{\upsilon}}_1\right) = \varphi'_{1,1,1} \left(\bar{\hat{\upsilon}}_1\right) \dot{\hat{\upsilon}}_1$, the expression of $\varphi'_{1,1,1} \left(\bar{\hat{\upsilon}}_j\right)$ is given in Remark 1, and $\Gamma_1 > 0$ is the positive design parameter.

By defining the tracking error as $\xi_1 = \hat{\upsilon}_1 - \upsilon_1^r$, where υ_1^r is the reference signal, the BLF (barrier Lyapunov function) is constructed as

$$L_{\eta_1} = \frac{\kappa_1^2}{\pi} \tan\left(\frac{\pi \eta_1^2}{2\kappa_1^2}\right), \tag{10}$$

where κ_1 is the given time-varying error-constraint bound and η_1 is the compensated tracking error defined by (14).

The virtual control signal υ_2^d is expressed as

$$\begin{aligned} \upsilon_2^d = g_1^{-1} \Bigg[& -\hat{\sigma}_1^{\mathrm{T}} \varphi_1\left(\bar{\hat{\upsilon}}_1\right) - \delta_1 + \dot{\upsilon}_1^r + \frac{\eta_1}{\kappa_1}\dot{\kappa}_1 - \frac{2\kappa_1\dot{\kappa}_1}{\pi\eta_1} \sin\left(\frac{\pi\eta_1^2}{2\kappa_1^2}\right) \cos\left(\frac{\pi\eta_1^2}{2\kappa_1^2}\right) \\ & - a_1 \frac{\cos^2\left(\frac{\pi\eta_1^2}{2\kappa_1^2}\right)}{\eta_1} \left(L_{\eta_1}\right)^{c_1} - b_1 \frac{\cos^2\left(\frac{\pi\eta_1^2}{2\kappa_1^2}\right)}{\eta_1} \left(L_{\eta_1}\right)^{c_2} - k_{11}\varsigma_1^2 - k_{12}\mathrm{var}\left(\varsigma_1, \bar{\varsigma}_1\right) \Bigg] \end{aligned} \tag{11}$$

with

$$\mathrm{var}\left(\varsigma_1, \bar{\varsigma}_1\right) = \begin{cases} \mathrm{sign}\left(\varsigma_1\right), & \text{if } \left|\varsigma_1\right| \geqslant \bar{\varsigma}_1, \\ \dfrac{3\varsigma_1}{2\bar{\varsigma}_1} - \dfrac{\varsigma_1^3}{2\bar{\varsigma}_1^3}, & \text{if } \left|\varsigma_1\right| < \bar{\varsigma}_1, \end{cases} \tag{12}$$

where $\dot{\upsilon}_1^r$ is the derivative of υ_1^r, $a_1 > 0$, $b_1 > 0$, $0 < c_1 < 1$, $c_2 > 1$, $k_{11} > 0$, and $k_{12} > 0$ are the positive design parameters; $0 \leqslant \bar{\varsigma}_1 \leqslant 1$ meets $|\varsigma_1| \leqslant 3\bar{\varsigma}_1$. The compensation signal ς_1 is given by (15).

The fixed-time filter is given as

$$m_{2,1}\dot{\upsilon}_2^r = -m_{2,2}\mathrm{sign}\left(\upsilon_2^r - \upsilon_2^d\right) - \mathrm{sig}^{c_1}\left(\upsilon_2^r - \upsilon_2^d\right) - \mathrm{sig}^{c_2}\left(\upsilon_2^r - \upsilon_2^d\right), \tag{13}$$

where $\mathrm{sig}^{c_1}\left(\upsilon_2^r - \upsilon_2^d\right) = \left\|\upsilon_2^r - \upsilon_2^d\right\|^{c_1} \mathrm{sign}\left(\upsilon_2^r - \upsilon_2^d\right)$, υ_2^r is the reference signal; $m_{2,1} > 0$ and $m_{2,2} > 0$ are the positive design parameters.

Define the tracking error as $\xi_2 = \hat{\upsilon}_2 - \upsilon_2^r$. The compensated tracking error is defined as

$$\eta_1 = \xi_1 - \varsigma_1. \tag{14}$$

Thus, the compensation signal ς_1 is obtained as

$$\dot{\varsigma}_1 = g_1\varsigma_2 + g_1\left(\upsilon_2^r - \upsilon_2^d\right) - k_{11}\varsigma_1^2 - k_{12}\mathrm{var}\left(\varsigma_1, \bar{\varsigma}_1\right), \tag{15}$$

where ς_2 is the compensation signal obtained from (24).

Step i $(i = 2, \cdots, n-1)$**:** Considering the identification of uncertainty $f_i\left(\bar{\upsilon}_i\right)$ and disturbance d_i, the SPIS is constructed as

$$\dot{\hat{\upsilon}}_i = \hat{\sigma}_i^{\mathrm{T}}\varphi_i\left(\bar{\hat{\upsilon}}_i\right) + g_i\hat{\upsilon}_{i+1} + \delta_i, \tag{16}$$

where $\hat{\upsilon}_i$ represents the identified state and δ_i is the RISE feedback term defined by (17).

Define the identification error and the filtered identification error as $\tilde{\upsilon}_i = \upsilon_i - \hat{\upsilon}_i$ and $s_i = \dot{\tilde{\upsilon}}_i + \alpha_i\tilde{\upsilon}_i$, respectively. The proposed term δ_i is expressed as

$$\delta_i = k_i\tilde{\upsilon}_i - k_i\tilde{\upsilon}_i\left(0\right) + \chi_i, \tag{17}$$

where the auxiliary signal χ_i is obtained from the following differential equation:

$$\dot{\chi}_i = \left(k_i\alpha_i + \gamma_i\right)\tilde{\upsilon}_i + \beta_i\mathrm{sign}\left(\tilde{\upsilon}_i\right) + \dot{g}_i\tilde{\upsilon}_{i+1} - g_i\alpha_{i+1}\tilde{\upsilon}_{i+1}, \tag{18}$$

where $k_i > 0$, $\alpha_i > 0$, $\gamma_i > 0$, $\beta_i > 0$, and $\alpha_{i+1} > 0$ are the positive design parameters.

The law for updating the fuzzy weight is expressed as

$$\dot{\hat{\sigma}}_i = \Gamma_i\dot{\varphi}_i\left(\bar{\hat{\upsilon}}_i\right)\tilde{\upsilon}_i, \tag{19}$$

where $\dot{\varphi}_i\left(\bar{\hat{\upsilon}}_i\right) = \left[\dot{\varphi}_{i,1}\left(\bar{\hat{\upsilon}}_i\right), \dot{\varphi}_{i,2}\left(\bar{\hat{\upsilon}}_i\right), \cdots, \dot{\varphi}_{i,\iota_i}\left(\bar{\hat{\upsilon}}_i\right)\right]^{\mathrm{T}}$, $\dot{\varphi}_{i,j}\left(\bar{\hat{\upsilon}}_i\right) = \sum_{k=1}^{i}\varphi'_{i,j,k}\left(\bar{\hat{\upsilon}}_i\right)\dot{\hat{\upsilon}}_i$, the expression of $\varphi'_{i,j,k}\left(\bar{\hat{\upsilon}}_j\right)$ is given in Remark 1, and $\Gamma_i > 0$ is the positive design parameter.

Define the tracking error as $\xi_i = \hat{\upsilon}_i - \upsilon_i^r$. The BLF is built as

$$L_{\eta_i} = \frac{\kappa_i^2}{\pi}\tan\left(\frac{\pi\eta_i^2}{2\kappa_i^2}\right), \tag{20}$$

where κ_i is the given time-varying error-constraint bound and η_i is the compensated tracking error defined by (23).

The virtual control signal υ_{i+1}^d is expressed as

$$\begin{aligned}\upsilon_{i+1}^d = g_i^{-1}\Bigg[&-\hat{\sigma}_i^{\mathrm{T}}\varphi_i\left(\bar{\hat{\upsilon}}_i\right) - \delta_i + \dot{\upsilon}_i^r + \frac{\eta_i}{\kappa_i}\dot{\kappa}_i - \frac{2\kappa_i\dot{\kappa}_i}{\pi\eta_i}\sin\left(\frac{\pi\eta_i^2}{2\kappa_i^2}\right)\cos\left(\frac{\pi\eta_i^2}{2\kappa_i^2}\right) - \frac{\cos\left(\frac{\pi\eta_i^2}{2\kappa_i^2}\right)}{\cos\left(\frac{\pi\eta_{i-1}^2}{2\kappa_{i-1}^2}\right)}g_{i-1}\xi_{i-1}\\ &-a_i\frac{\cos^2\left(\frac{\pi\eta_i^2}{2\kappa_i^2}\right)}{\eta_i}\left(L_{\eta_i}\right)^{c_1} - b_i\frac{\cos^2\left(\frac{\pi\eta_i^2}{2\kappa_i^2}\right)}{\eta_i}\left(L_{\eta_i}\right)^{c_2} - k_{i1}\varsigma_i^2 - k_{i2}\mathrm{var}\left(\varsigma_i, \bar{\varsigma}_i\right)\Bigg],\end{aligned} \tag{21}$$

where $a_i > 0$, $b_i > 0$, $k_{i1} > 0$, and $k_{i2} > 0$ are the positive design parameters; $0 \leqslant \bar{\varsigma}_i \leqslant 1$ meets $|\varsigma_i| \leqslant 3\bar{\varsigma}_i$. The compensation signal ς_i is given by (24).

The fixed-time filter is expressed as

$$m_{i+1,1}\dot{\upsilon}_{i+1}^r = -m_{i+1,2}\mathrm{sign}\left(\upsilon_{i+1}^r - \upsilon_{i+1}^d\right) - \mathrm{sig}^{c_1}\left(\upsilon_{i+1}^r - \upsilon_{i+1}^d\right) - \mathrm{sig}^{c_2}\left(\upsilon_{i+1}^r - \upsilon_{i+1}^d\right), \tag{22}$$

where υ_{i+1}^r is the reference signal, $m_{i+1,1} > 0$ and $m_{i+1,2} > 0$ are the positive design parameters.

The compensated tracking error is defined as

$$\eta_i = \xi_i - \varsigma_i. \tag{23}$$

Thus, the compensation signal ς_i is obtained as

$$\dot{\varsigma}_i = g_i\left(\upsilon_{i+1}^r - \upsilon_{i+1}^d\right) + g_i\varsigma_{i+1} - \frac{\cos\left(\frac{\pi\eta_i^2}{2\kappa_i^2}\right)}{\cos\left(\frac{\pi\eta_{i-1}^2}{2\kappa_{i-1}^2}\right)}g_{i-1}\varsigma_{i-1} - k_{i1}\varsigma_i^2 - k_{i2}\mathrm{var}\left(\varsigma_i, \bar{\varsigma}_i\right). \tag{24}$$

Step n: Considering the identification of uncertainty $f_n(\bar{\upsilon}_n)$ and disturbance d_n, the SPIS is constructed as

$$\dot{\hat{\upsilon}}_n = \hat{\sigma}_n^{\mathrm{T}} \varphi_n\left(\bar{\hat{\upsilon}}_n\right) + g_n \mu + \delta_n, \tag{25}$$

where $\hat{\upsilon}_n$ represents the identified state and δ_n is the RISE feedback term defined by (17).

Define the identification error and the filtered identification error as $\tilde{\upsilon}_n = \upsilon_n - \hat{\upsilon}_n$ and $s_n = \dot{\tilde{\upsilon}}_n + \alpha_n \tilde{\upsilon}_n$, respectively. The proposed term δ_n is expressed as

$$\delta_n = k_n \tilde{\upsilon}_n - k_n \tilde{\upsilon}_n(0) + \chi_n, \tag{26}$$

where the auxiliary signal χ_n is obtained from the following differential equation:

$$\dot{\chi}_n = \left(k_n \alpha_n + \gamma_n\right) \tilde{\upsilon}_n + \beta_n \mathrm{sign}\left(\tilde{\upsilon}_n\right), \tag{27}$$

where $k_n > 0$, $\alpha_n > 0$, $\gamma_n > 0$, and $\beta_n > 0$ are the positive design parameters.

The law for updating the fuzzy weight is expressed as

$$\dot{\hat{\sigma}}_n = \Gamma_n \dot{\varphi}_n\left(\bar{\hat{\upsilon}}_n\right) \tilde{\upsilon}_n, \tag{28}$$

where $\dot{\varphi}_n\left(\bar{\hat{\upsilon}}_n\right) = \left[\dot{\varphi}_{n,1}\left(\bar{\hat{\upsilon}}_n\right), \dot{\varphi}_{n,2}\left(\bar{\hat{\upsilon}}_n\right), \cdots, \dot{\varphi}_{n,\iota_n}\left(\bar{\hat{\upsilon}}_n\right)\right]^{\mathrm{T}}$, $\dot{\varphi}_{n,j}\left(\bar{\hat{\upsilon}}_n\right) = \sum_{k=1}^{n} {\varphi'}_{n,j,k}\left(\bar{\hat{\upsilon}}_n\right) \dot{\hat{\upsilon}}_n$, the expression of ${\varphi'}_{n,j,k}\left(\bar{\hat{\upsilon}}_j\right)$ is given in Remark 1, and $\Gamma_n > 0$ is the positive design parameter.

Define the tracking error as $\xi_n = \hat{\upsilon}_n - \upsilon_n^r$. The BLF is built as

$$L_{\eta_n} = \frac{\kappa_n^2}{\pi} \tan\left(\frac{\pi \eta_n^2}{2\kappa_n^2}\right), \tag{29}$$

where κ_n is the given time-varying error-constraint bound and η_n is the compensated tracking error defined by (31).

The control input is expressed as

$$\begin{aligned} \mu = g_n^{-1} \Bigg[& -\hat{\sigma}_n^{\mathrm{T}} \varphi_n\left(\bar{\hat{\upsilon}}_n\right) - \delta_n + \dot{\upsilon}_n^r + \frac{\eta_n}{\kappa_n}\dot{\kappa}_n - \frac{2\kappa_n \dot{\kappa}_n}{\pi \eta_n} \sin\left(\frac{\pi \eta_n^2}{2\kappa_n^2}\right) \cos\left(\frac{\pi \eta_n^2}{2\kappa_n^2}\right) - \frac{\cos\left(\frac{\pi \eta_n^2}{2\kappa_n^2}\right)}{\cos\left(\frac{\pi \eta_{n-1}^2}{2\kappa_{n-1}^2}\right)} g_{n-1} \xi_{n-1} \\ & - a_n \frac{\cos^2\left(\frac{\pi \eta_n^2}{2\kappa_n^2}\right)}{\eta_n} \left(L_{\eta_n}\right)^{c_1} - b_n \frac{\cos^2\left(\frac{\pi \eta_n^2}{2\kappa_n^2}\right)}{\eta_n} \left(L_{\eta_n}\right)^{c_2} - k_{n1} \varsigma_n^2 - k_{n2} \mathrm{var}\left(\varsigma_n, \bar{\varsigma}_n\right) \Bigg], \end{aligned} \tag{30}$$

where $a_n > 0$, $b_n > 0$, $k_{n1} > 0$, and $k_{n2} > 0$ are the positive parameters; $0 \leqslant \bar{\varsigma}_n \leqslant 1$ meets $|\varsigma_n| \leqslant 3\bar{\varsigma}_n$. The compensation signal ς_n is given by (32).

The compensated tracking error is defined as

$$\eta_n = \xi_n - \varsigma_n. \tag{31}$$

Thus, the compensation signal ς_n is obtained as

$$\dot{\varsigma}_n = -\frac{\cos\left(\frac{\pi \eta_n^2}{2\kappa_n^2}\right)}{\cos\left(\frac{\pi \eta_{n-1}^2}{2\kappa_{n-1}^2}\right)} g_{n-1} \varsigma_{n-1} - k_{n1} \varsigma_n^2 - k_{n2} \mathrm{var}\left(\varsigma_n, \bar{\varsigma}_n\right). \tag{32}$$

Remark 2. The function $\mathrm{var}\left(\varsigma_i, \bar{\varsigma}_i\right)$ is introduced to serve as an equivalent to the sign function, thereby circumventing the singularity problem inherent in the fixed-time filters (13) and (22).

Remark 3. The original system is subject to dynamic uncertainties f_i and external disturbances d_i. The objective of incorporating feedforward information into the controller design is to reduce adverse impacts on the system performance. However, because the exact values of these uncertainties and disturbances are typically unknown, direct verification of the correctness of the feedforward information is impractical. Consequently, an identification system is developed using the original model structure in conjunction with estimates of the uncertainties and disturbances. If the states of the identification system align closely with those of the original system, the accuracy of the feedforward information can be indirectly inferred.

Remark 4. Define the auxiliary functions as

$$\begin{cases} s_{i1} = -\dot{\hat{\sigma}}_i^{\mathrm{T}} \varphi_i\left(\bar{\hat{\upsilon}}_i\right) + \alpha_i \dot{\tilde{\upsilon}}_i + \sigma_i^{*\mathrm{T}} \dot{\varphi}_i\left(\bar{\hat{\upsilon}}_i\right), \\ s_{i2} = \dot{\varepsilon}_i + \dot{d}_i + \sigma_i^{*\mathrm{T}} \dot{\varphi}_i\left(\bar{\upsilon}_i\right) - \sigma_i^{*\mathrm{T}} \dot{\varphi}_i\left(\bar{\upsilon}_i\right), \\ s_{i3} = \tilde{\sigma}_i^{\mathrm{T}} \dot{\varphi}_i\left(\bar{\upsilon}_i\right), \\ \hat{s}_{i3} = \tilde{\sigma}_i^{\mathrm{T}} \dot{\varphi}_i\left(\bar{\hat{\upsilon}}_i\right). \end{cases} \tag{33}$$

From (6)–(8), (16)–(18), and (25)–(27), $\dot{s}_i$ is calculated as

$$\begin{cases} \dot{s}_i = s_{i1} + s_{i2} + \hat{s}_{i3} + g_i s_{i+1} - k_i s_i - \gamma_i \tilde{\upsilon}_i - \beta_i \mathrm{sign}\left(\tilde{\upsilon}_i\right), \\ \dot{s}_n = s_{n1} + s_{n2} + \hat{s}_{n3} - k_n s_n - \gamma_n \tilde{\upsilon}_n - \beta_n \mathrm{sign}\left(\tilde{\upsilon}_n\right). \end{cases} \tag{34}$$

Remark 5. The separation of terms in (33) is characteristic of the RISE strategy and provides a foundation for the boundary partitioning and stability analysis using (37) and (38). Specifically, the term s_1 is related to the system errors s_i and $\tilde{\upsilon}_i$. The term s_{i2} includes bounded components, such as $\dot{\varepsilon}_i$ and σ_i^*, which are subsequently cancelled by the RISE term δ_i. Additionally, the term s_{i3} involves components associated with the signal $\tilde{\sigma}_i$, compensated through the fuzzy update law (19) and the RISE term δ_i.

4 Stability analysis

4.1 Stability analysis for SPIS

Theorem 1. Considering the model of the dynamics of the strict-feedback nonlinear system (1), if the SPISs (6), (16), and (25) are built with the RISE feedback terms (7), (17), and (26) as well as the update laws of the fuzzy weights (9), (19), and (28), the error signals s_i, $\tilde{\upsilon}_i$, and $\tilde{\sigma}_i$ in (35) are bounded.

Proof. The Lyapunov function is given as

$$L_s = \sum_{i=1}^{n} \frac{1}{2} s_i^2 + \frac{1}{2} \gamma_i \tilde{\upsilon}_i^2 + \frac{1}{2} \alpha_i \tilde{\sigma}_i^{\mathrm{T}} \Gamma_i^{-1} \tilde{\sigma}_i + L_{oi}, \tag{35}$$

where L_{oi} is obtained as

$$\dot{L}_{oi} = -s_i\left(s_{i2} - \beta_i \mathrm{sign}\left(\tilde{\upsilon}_i\right)\right) - \dot{\tilde{\upsilon}}_i^{\mathrm{T}} s_{i3} + \beta_{i1} \lambda_{i2}\left(\|\zeta_i\|\right)\left|\tilde{\upsilon}_i\right| \tag{36}$$

with $\zeta_i = \left[s_i^{\mathrm{T}} \tilde{\upsilon}_i^{\mathrm{T}}\right]^{\mathrm{T}}$, $L_{oi}(0) = \beta_i \left|\tilde{\upsilon}_i(0)\right| - \tilde{\upsilon}_i(0)\left[s_{i2}(0) + s_{i3}(0)\right]$.

From Assumptions 1–2, (19), and (33), the function s_{i1} is bounded by

$$\left|s_{i1}\right| \leqslant \lambda_{i1}\left(\|\zeta_i\|\right)\|\zeta_i\|, \tag{37}$$

where $\lambda_{i1}\left(\|\zeta_i\|\right) \in \Re^+$ is the globally invertible and nondecreasing function. Eqs. (33) and (34) are bounded with [39]

$$\begin{cases} \left|s_{i2}\right| \leqslant \bar{s}_{i2}, \quad \left|s_{i3}\right| \leqslant \bar{s}_{i3}, \\ \left|\dot{s}_{i2} + \dot{s}_{i3}\right| \leqslant \bar{s}_{i4} + \bar{s}_{i5} \lambda_{i2}\left(\|\zeta_i\|\right)\|\zeta_i\|, \\ \left|\dot{\tilde{\upsilon}}_i \tilde{s}_{i3}\right| \leqslant \bar{s}_{i6} \tilde{\upsilon}_i^2 + \bar{s}_{i7} s_i^2, \end{cases} \tag{38}$$

where $\tilde{s}_{i3} = s_{i3} - \hat{s}_{i3}$, $\bar{s}_{il} > 0$ is a computable constant $l = 2, \cdots, 7$, and $\lambda_{i3}\left(\|\zeta_i\|\right) \in \Re^+$ is a globally invertible and nondecreasing function.

The Lyapunov function in (35) is positive definite once the following sufficient conditions are satisfied:

$$\begin{cases} \beta_i > \max\left(\bar{s}_{i2} + \bar{s}_{i3}, \bar{s}_{i2} + \dfrac{\bar{s}_{i4}}{\alpha_i}\right), \\ \beta_{i1} > \bar{s}_{i5}. \end{cases} \tag{39}$$

Considering the Young's inequality and Assumption 1, the following inequality can be obtained as

$$g_i s_i s_{i+1} \leqslant \frac{1}{2} \kappa_{si} \bar{g}_i s_i^2 + \frac{1}{2\kappa_{si}} \bar{g}_i s_{i+1}^2, \tag{40}$$

where $\kappa_{si} > 0$ is the positive parameter.

Thus, the derivative of L_s is computed as

$$\begin{aligned}
\dot{L}_s &= \sum_{i=1}^{n} s_i \left(s_{i1} + s_{i2} + \hat{s}_{i3} - k_i s_i - \gamma_i \tilde{\upsilon}_i - \beta_i \mathrm{sign}\left(\tilde{\upsilon}_i\right)\right) + \tilde{\upsilon}_i \gamma_i \left(s_i - \alpha_i \tilde{\upsilon}_i\right) - \dot{\tilde{\upsilon}}_i^{\mathrm{T}} s_{i3} \\
&\quad - \alpha_i \tilde{\sigma}_i^{\mathrm{T}} \dot{\varphi}_i\left(\bar{\tilde{\upsilon}}_i\right) \tilde{\upsilon}_i - s_i \left(s_{i2} - \beta_i \mathrm{sign}\left(\tilde{\upsilon}_i\right)\right) + \beta_{i1} \lambda_{i2}\left(\|\zeta_i\|\right) \|\zeta_i\| \left|\tilde{\upsilon}_i\right| + \sum_{i=1}^{n-1} g_i s_i s_{i+1} \\
&= -\left(k_1 - \frac{1}{2}\kappa_{s1}\bar{g}_1\right) s_1^2 - \left(k_n - \frac{1}{2\kappa_{sn-1}}\bar{g}_{n-1}\right) s_n^2 - \sum_{i=2}^{n-1}\left(k_i - \frac{1}{2}\kappa_{si}\bar{g}_i - \frac{1}{2\kappa_{si-1}}\bar{g}_{i-1}\right) s_i^2 \\
&\quad + \sum_{i=1}^{n} -\alpha_i \gamma_i \tilde{\upsilon}_i^2 - \dot{\tilde{\upsilon}}_i^{\mathrm{T}} \tilde{s}_{i3} + s_i s_{i1} + \beta_{i1}\lambda_{i2}\left(\|\zeta_i\|\right)\left|\tilde{\upsilon}_i\right| \\
&\leqslant \sum_{i=1}^{n} -\bar{k}_i s_i^2 - \alpha_i \gamma_i \tilde{\upsilon}_i^2 + \bar{s}_{i6}\tilde{\upsilon}_i^2 + \bar{s}_{i7} s_i^2 + \lambda_{i1}\left(\|\zeta_i\|\right)\|\zeta_i\| \left|s_i\right| + \beta_{i1}\lambda_{i2}\left(\|\zeta_i\|\right)\|\zeta_i\|\left|\tilde{\upsilon}_i\right|,
\end{aligned} \tag{41}$$

where $\bar{k}_i = \min\left(k_1 - \frac{1}{2}\kappa_{s1}\bar{g}_1, k_i - \frac{1}{2}\kappa_{si}\bar{g}_i - \frac{1}{2\kappa_{si-1}}\bar{g}_{i-1}, k_n - \frac{1}{2\kappa_{sn-1}}\bar{g}_{n-1}\right)$.

The following inequalities hold:

$$\begin{cases}
\lambda_{i1}\left(\|\zeta_i\|\right)\|\zeta_i\|\left|s_i\right| \leqslant \dfrac{\lambda_{i1}^2\left(\|\zeta_i\|\right)\|\zeta_i\|^2}{4\omega_{i1}} + \omega_{i1} s_i^2, \\
\beta_{i1}\lambda_{i2}\left(\|\zeta_i\|\right)\|\zeta_i\|\left|\tilde{\upsilon}_i\right| \leqslant \dfrac{\beta_{i1}^2\lambda_{i2}^2\left(\|\zeta_i\|\right)\|\zeta_i\|^2}{4\alpha_i\omega_{i2}} + \alpha_i\omega_{i2}\tilde{\upsilon}_i^2,
\end{cases} \tag{42}$$

where $\omega_{i1} > 0$ and $\omega_{i2} > 0$ are positive constants.

By substituting into (42), the signal $\dot{L}_s$ can be rewritten as

$$\dot{L}_s \leqslant \sum_{i=1}^{n} -\left(\bar{k}_i - \omega_{i1} - \bar{s}_{i7}\right) s_i^2 - \left(\alpha_i\gamma_i - \alpha_i\omega_{i2} - \bar{s}_{i6}\right)\tilde{\upsilon}_i^2 + \frac{\lambda_{i1}^2\left(\|\zeta_i\|\right)\|\zeta_i\|^2}{4\omega_{i1}} + \frac{\beta_{i1}^2\lambda_{i2}^2\left(\|\zeta_i\|\right)\|\zeta_i\|^2}{4\alpha_i\omega_{i2}}. \tag{43}$$

The parameters are chosen to satisfy the sufficient conditions as follows:

$$\begin{cases}
k_1 - \dfrac{1}{2}\kappa_{s1}\bar{g}_1 > 0, \\
k_i - \dfrac{1}{2}\kappa_{si}\bar{g}_i - \dfrac{1}{2\kappa_{si-1}}\bar{g}_{i-1} > 0, \\
k_n - \dfrac{1}{2\kappa_{sn-1}}\bar{g}_{n-1} > 0, \\
\bar{k}_i - \omega_{i1} - \bar{s}_{i7} > 0, \\
\alpha_i\gamma_i - \alpha_i\omega_{i2} - \bar{s}_{i6} > 0.
\end{cases} \tag{44}$$

The derivative of L_s is arranged as

$$\dot{L}_s \leqslant -K_1 \sum_{i=1}^{n} s_i^2 - K_2 \sum_{i=1}^{n} \tilde{\upsilon}_i^2 + \sum_{i=1}^{n} \frac{\lambda_i^2\|\zeta_i\|^2}{4\omega_i}, \tag{45}$$

where $K_1 = \min\left(\bar{k}_i - \omega_{i1} - \bar{s}_{i7}\right)$, $K_2 = \min\left(\alpha_i\gamma_i - \alpha_i\omega_{i2} - \bar{s}_{i6}\right)$, $\omega_i = \min\left(\frac{1}{\omega_{i1}}, \frac{\beta_{i1}}{\alpha_i\omega_{i2}}\right)$, and $\lambda_i^2 = \lambda_{i1}^2\left(\|\zeta_i\|\right) + \lambda_{i2}^2\left(\|\zeta_i\|\right)$.

The error signals in (35) are semi-globally stable [40] and the region of attraction can be expanded by increasing the design parameter ω_i.

4.2 Stability analysis for controller

Theorem 2. Considering the model of the dynamics of the strict-feedback nonlinear system (1), if the virtual control signals (11) and (21), as well as the control input (30), are proposed, the error signal η_i will converge in a fixed time, and the asymmetric time-varying state constraint κ_i will always be satisfied.

Proof. The Lyapunov function is selected as

$$L_\eta = \sum_{i=1}^{n} L_{\eta i}. \tag{46}$$

From (10)–(15), (20)–(24), and (29)–(32), $\dot{L}_\eta$ is computed as

$$\begin{aligned}\dot{L}_\eta &= \sum_{i=1}^{n}\left[\frac{2\kappa_i\dot{\kappa}_i}{\pi}\tan\left(\frac{\pi\eta_i^2}{2\kappa_i^2}\right)+\sec^2\left(\frac{\pi\eta_i^2}{2\kappa_i^2}\right)\left(\eta_i\dot{\eta}_i-\frac{\dot{\kappa}_i}{\kappa_i}\eta_i^2\right)\right]\\ &= -\sum_{i=1}^{n}\left(a_i(L_{\eta_i})^{c_1}+b_i(L_{\eta_i})^{c_2}\right)\\ &\leqslant -a(L_\eta)^{c_1}-bn^{1-c_2}(L_\eta)^{c_2},\end{aligned} \tag{47}$$

where $a=\min(a_i)$ and $b=\min(b_i)$.

According to Theorem 1 in [41], Lemma 1 in [42], and Eq. (47), the error signal η_i converges in a fixed time $T_1 \leqslant \frac{1}{a(1-c_1)}+\frac{n^{c_2-1}}{b(c_2-1)}$, where the convergence time is reduced by increasing the parameters a and b. Furthermore, η_i is constrained within the predetermined function κ_i.

Thus, the Lyapunov function L_ς is chosen as

$$L_\varsigma = \sum_{i=1}^{n}\frac{1}{2}\varsigma_i^2. \tag{48}$$

Combining (15), (24), (32), and the Lemma 5 in [43], the derivative of L_ς is solved as

$$\begin{aligned}\dot{L}_\varsigma &= \sum_{i=1}^{n} g_i\left(\upsilon_{i+1}^r-\upsilon_{i+1}^d\right)\varsigma_i+\sum_{i=1}^{n-1}g_i\varsigma_i\varsigma_{i+1}-\sum_{i=2}^{n}\frac{\cos\left(\frac{\pi\eta_i^2}{2\kappa_i^2}\right)}{\cos\left(\frac{\pi\eta_{i-1}^2}{2\kappa_{i-1}^2}\right)}g_{i-1}\varsigma_{i-1}\varsigma_i-k_{i1}\varsigma_i^3-k_{i2}\varsigma_i\mathrm{var}\left(\varsigma_n,\bar{\varsigma}_n\right)\\ &\leqslant \sum_{i=1}^{n}\left[g_i\left(\upsilon_{i+1}^r-\upsilon_{i+1}^d\right)\varsigma_i\right]-2\sqrt{2}K_{C1}\left(\sum_{i=1}^{n}\frac{1}{2}\varsigma_i^2\right)^{\frac{3}{2}}-\sqrt{2}K_{C2}\left(\sum_{i=1}^{n}\frac{1}{2}\varsigma_i^2\right)^{\frac{1}{2}}+\frac{K_3}{4}+K_3\sum_{i=1}^{n}\frac{1}{2}\varsigma_i^2,\end{aligned} \tag{49}$$

where $K_{C1}=\min\{k_{11},\cdots,k_{n1}\}$, $K_{C2}=\min\{k_{12},\cdots,k_{n2}\}$, $K_3=\min\left\{\sqrt{2}k_{12},\cdots,\sqrt{2}k_{\tau 2}\right\}$, and τ is the number of errors ς_i meeting $|\varsigma_i|\geqslant\bar{\varsigma}_i$.

Considering the stability of the filter in [44], the filter error $\left(\upsilon_{i+1}^r-\upsilon_{i+1}^d\right)$ is bounded and stable in fixed time. Thus, under Assumption 1 and Lemma 3 in [45], $\dot{L}_\varsigma$ can be written as

$$\begin{aligned}\dot{L}_\varsigma &\leqslant \sum_{i=1}^{n}\bar{g}_i\epsilon_i\varsigma_i-2\sqrt{2}K_{C1}\left(\sum_{i=1}^{n}\frac{1}{2}\varsigma_i^2\right)^{\frac{3}{2}}-\sqrt{2}K_{C2}\left(\sum_{i=1}^{n}\frac{1}{2}\varsigma_i^2\right)^{\frac{1}{2}}+\frac{K_3}{4}+K_3\left[\frac{1}{3}K_4+\frac{2}{3}K_4^{-\frac{1}{2}}\left(\sum_{i=1}^{n}\frac{1}{2}\varsigma_i^2\right)^{\frac{3}{2}}\right]\\ &\leqslant -\sqrt{2}\left(K_{C2}-n^{\frac{1}{2}}\bar{g}\epsilon\right)L_\varsigma^{\frac{1}{2}}-\left(2\sqrt{2}K_{C1}-\frac{2}{3}K_3K_4^{-\frac{1}{2}}\right)L_\varsigma^{\frac{3}{2}}+\frac{K_3}{4}+\frac{1}{3}K_3K_4,\end{aligned} \tag{50}$$

where ϵ_i is the existing constant, $\bar{g}=\max\{\bar{g}_i,\cdots,\bar{g}_n\}$, $\epsilon=\max\{\epsilon_i,\cdots,\epsilon_n\}$, and $K_4>0$ is the given constant.

As stated in [46], if the parameters meet the following conditions:

$$\begin{cases} K_{C1}>\dfrac{1}{3\sqrt{2}}K_3K_4^{-\frac{1}{2}},\\ K_{C2}>n^{\frac{1}{2}}\bar{g}\epsilon. \end{cases} \tag{51}$$

Then L_ς is stable in fixed time and the convergence time satisfies $T_2 \leqslant \frac{2}{\sqrt{2}(K_{C2}-n^{\frac{1}{2}}\bar{g}\epsilon)K_5}+\frac{2}{(2\sqrt{2}K_{C1}-\frac{2}{3}K_3K_4^{-\frac{1}{2}})K_5}$.

Define the tracking error of system (1) as $e_i=\upsilon_i-\upsilon_i^r=\eta_i+\varsigma_i+\tilde{\upsilon}_i$. Because the compensated tracking error η_i, compensation signal ς_i, and identification error $\tilde{\upsilon}_i$ converge, the tracking error satisfies $e_i\leqslant\bar{e}_i$. This completes the proof.

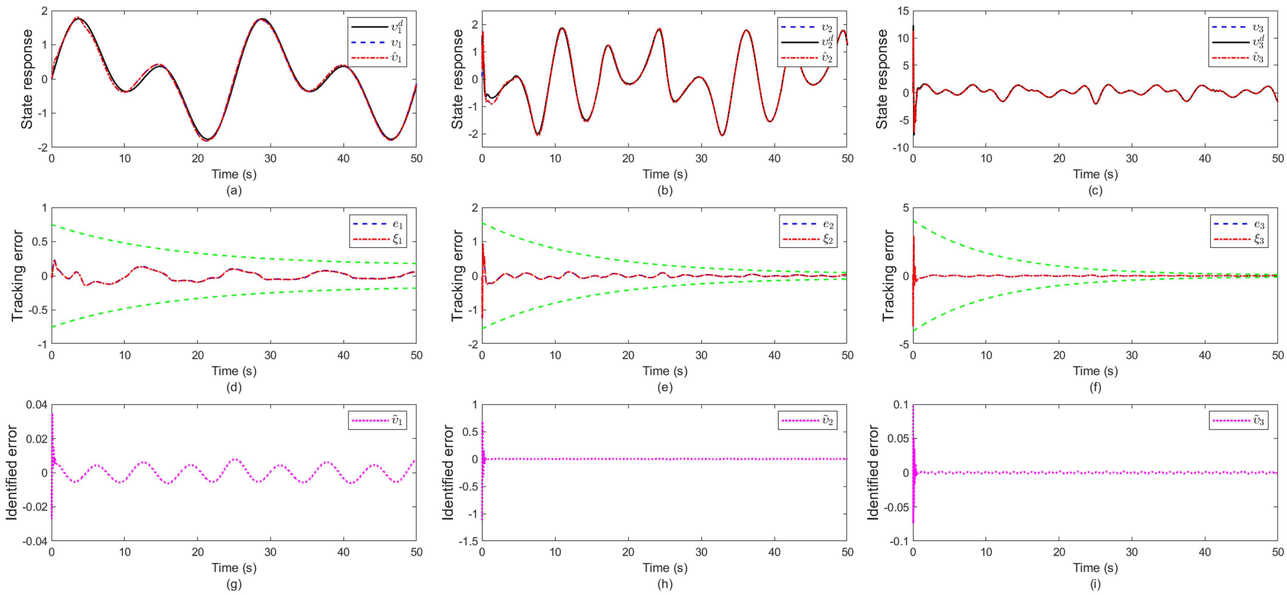

Figure 2 (Color online) System status tracking response and identification performance for Case 1. Tracking responses of (a) υ_1, (b) υ_2, and (c) υ_3; tracking errors (d) e_1 and ξ_1, (e) e_2 and ξ_2, and (f) e_3 and ξ_3; identification errors (g) $\tilde{\upsilon}_1$, (h) $\tilde{\upsilon}_2$, and (i) $\tilde{\upsilon}_3$.

5 Simulation

In this section, two distinct nonlinear systems are utilized as simulation examples to demonstrate the control and learning performance of the proposed method. The nonlinear systems employed in Cases 1–4 are third-order systems subject to dynamic uncertainties and external disturbances. In Case 1, a time-varying disturbance satisfying Assumption 1 is considered. Case 2 investigates the influence of various key design parameters on the stability and performance of the system by establishing multiple parameter sets. The results of the simulation are compared with those employing conventional intelligent control and sliding-mode control methods in Case 3. Case 4 examines the impact of noise disturbances. In Case 5, the attitude dynamics of an aircraft model is used for the simulation system, considering the effects of the time-varying moment of inertia and wind disturbances.

5.1 Simulation of third-order system

The third-order nonlinear system is given as

$$\begin{cases} \dot{\upsilon}_1 = \sin(\upsilon_1) + \left(1+\upsilon_1^2\right)\upsilon_2 + d_1, \\ \dot{\upsilon}_2 = \sin(\upsilon_2) + \upsilon_1\upsilon_2 + 2\upsilon_3 + d_2, \\ \dot{\upsilon}_3 = \sin(\upsilon_1\upsilon_2\upsilon_3) + \upsilon_1^2\upsilon_3 + [3 + 0.2\cos(\upsilon_1) + 0.5\sin(\upsilon_2)\sin(\upsilon_1)]\,u + d_3. \end{cases} \tag{52}$$

The reference command is specified as $\upsilon_1^r = 0.5(\sin(t) + \sin(0.5t))$ and the initial system states are selected as $\upsilon_1(0) = 0$, $\upsilon_2(0) = 0.1$, and $\upsilon_3(0) = 0.1$. The boundaries of the states are set as $\kappa_1 = 0.5e^{-0.05t}$, $\kappa_2 = 1.5e^{-0.07t}$, and $\kappa_3 = 4e^{-0.09t}$. In the controller design, the parameters of the identifier are set as $k_i = 20$, $\alpha_i = 5$, $\gamma_i = 200$, and $\beta_i = 10$, $\Gamma_i = 0.1$. The parameters of the control law are denoted by $a_i = 30$, $b_i = 15$, $c_1 = 0.5$, $c_2 = 2.2$, $k_{i1} = 0.1$, $k_{i2} = 0.3$, $m_{i1} = 0.5$, $m_{i2} = 0.01$, and $i = (1, 2, 3)$.

Case 1: Time-varying bounded disturbance with second-order differentiability. The external disturbances are modeled as $d_1 = 1.5\sin(t)$, $d_2 = \cos(2t)$, and $d_3 = \sin(5t)$. The simulation results are illustrated in Figures 2 and 3. The tracking response and identification performance of the system states are depicted in Figure 2. The system states accurately track the desired commands, where the steady-state values of tracking errors e_1, e_2, and e_3 fluctuate within intervals of $[-0.008, 0.0133]$, $[-0.012, 0.036]$, and $[-0.022, 0.016]$, respectively. The output states $\hat{\upsilon}_1$ and $\hat{\upsilon}_2$, $\hat{\upsilon}_3$ of the identification model closely match the system states υ_1, υ_2, and υ_3 in the dynamic model, where the identification errors $\tilde{\upsilon}_1$, $\tilde{\upsilon}_2$, and $\tilde{\upsilon}_3$ are less than 0.001. The identification model can be used as a proxy model of the original system (52) for controller design. As shown in Figure 3, the norm curve of the fuzzy weight tends toward gradual convergence.

Case 2: Impact of different key design parameters. Based on the analysis presented in Subsection 4.2, to guarantee the stability of the closed-loop control system, the parameters should initially be set as $a_i > 0$, $b_i > 0$,

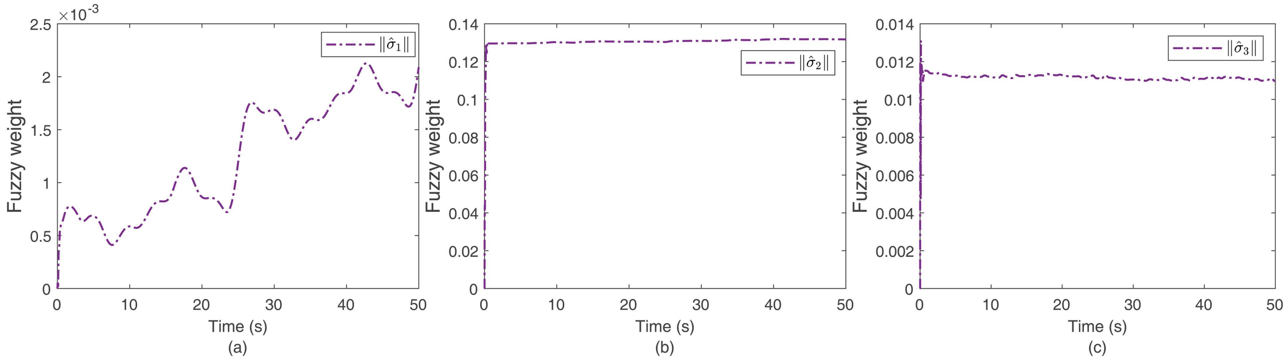

Figure 3 (Color online) Norm of fuzzy weight $\hat{\sigma}_i$ for Case 1. (a) $\|\hat{\sigma}_1\|$; (b) $\|\hat{\sigma}_2\|$; (c) $\|\hat{\sigma}_3\|$.

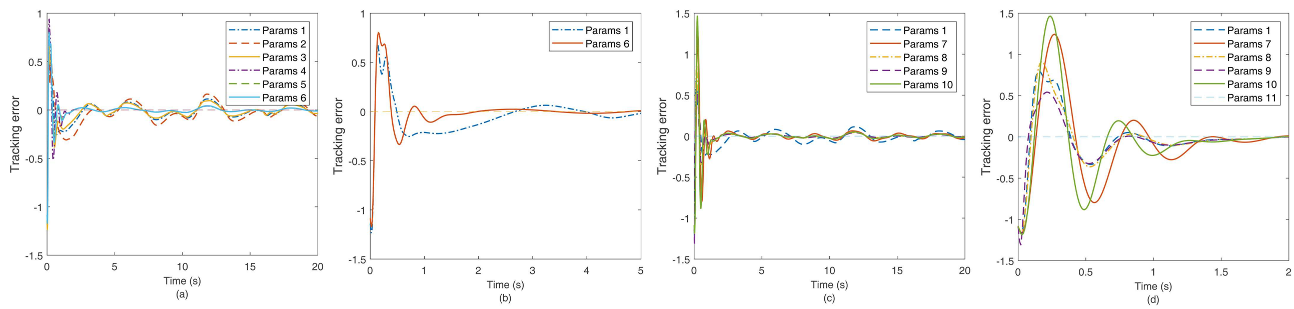

Figure 4 (Color online) Tracking errors e_2 using ten parameter sets. (a) e_2 under Params 1–6; (b) e_2 for Params 1 and 6 within $[0, 5]$ s; (c) e_2 under Params 1 and 7–10; (d) e_2 for Params 1 and 7–11 within $[0, 2]$ s;

Table 1 Ten parameter sets.

	a_i	b_i	c_1	c_2	k_i	α_i	γ_i		a_i	b_i	c_1	c_2	k_i	α_i	γ_i
Params 1	10	5	0.7	1.2	20	5	200	Params 6	30	15	0.5	2.2	20	5	200
Params 2	5	2	0.7	1.2	20	5	200	Params 7	10	5	0.7	1.2	20	1	10
Params 3	30	15	0.7	1.2	20	5	200	Params 8	10	5	0.7	1.2	20	25	10
Params 4	10	5	0.5	2.2	20	5	200	Params 9	10	5	0.7	1.2	30	5	200
Params 5	5	2	0.5	2.2	20	5	200	Params 10	10	5	0.7	1.2	10	5	200

$0 < c_1 < 1$, and $c_2 > 1$. Additionally, parameters k_{i1} and k_{i2} should be selected to satisfy the inequality (51), while parameters k_i, α_i, and γ_i must fulfill the conditions $\bar{k}_i - \omega_{i1} - \bar{s}_{i7} > 0$ and $\alpha_i\gamma_i - \alpha_i\omega_{i2} - \bar{s}_{i6} > 0$.

Furthermore, according to (45), (47), and (50), the convergence time of the tracking error, denoted by $T = \min\{T_1, T_2\}$, decreases with increasing a_i, b_i, and c_2, and decreasing c_1. The control accuracy is influenced by both the state estimation error and the control gains. The former is primarily affected by parameters k_i, α_i, and γ_i, whereas the latter predominantly depends on parameters a_i and b_i.

Ten different groups of design parameters are presented in Table 1. The corresponding tracking error e_2 is illustrated in Figure 4. When c_1 is reduced from 0.7 to 0.5 and c_2 is increased from 1.2 to 2.2, the convergence time decreases from 4.8 to 1.95 s. Compared to their effect on the convergence time, variations in parameters a_i and b_i predominantly influence the dynamic response characteristics of the tracking error. Furthermore, when parameter k_i is increased, the overshoot of the tracking error decreases from 0.79 to 0.51, whereas reductions in α_i and k_i lead to nearly a twofold increase in the oscillation amplitude of the tracking error.

Case 3: Comparison of simulation results with those employing intelligent control and sliding-mode control. The model-based learning controller proposed in this study is referred to as "IMLC". The neural learning adaptive robust controller in [47] used for comparison is denoted by "NARC" and the disturbance observer-based adaptive neural control in [48] is termed "DOAC".

The status tracking response curve in Figure 5 presents a comparison of the simulation results with those obtained using the different controllers. Faced with the same uncertainty and time-varying disturbance, the tracking error of the system is larger when the NARC method is used, whereas the tracking error of the system converges slowly with the DOAC method. The IMLC controller guarantees both convergence speed and steady-state accuracy. This performance difference arises because the time-varying external disturbance d_i affects the estimation accuracy of

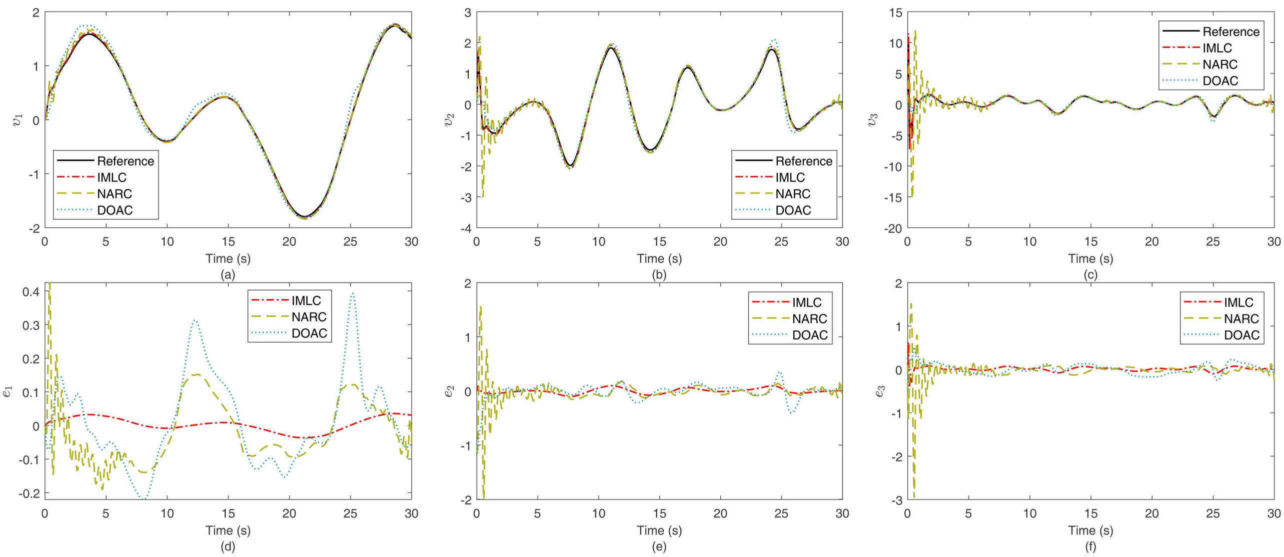

Figure 5 (Color online) System status tracking responses for Case 3. Tracking responses of (a) υ_1, (b) υ_2, and (c) υ_3; tracking errors (d) e_1, (e) e_2, and (f) e_3.

the network using the NARC method, whereas the design framework of the DOAC method ignores the impact of the convergence speed.

Case 4: White Gaussian noise disturbance. The disturbances are modeled as white Gaussian noise using a covariance matrix $R = 0.1$. The boundaries of the states are selected as $\kappa_1 = 0.6e^{-0.06t} + 0.15$, $\kappa_2 = 1.5e^{-0.07t} + 0.5$, and $\kappa_3 = 8e^{-0.09t} + 1.2$. The simulation results are presented in Figures 6–8. Figures 6(a)–(c) show that both the system states and identified states track the desired commands in the presence of interference from white Gaussian noise. The tracking performance is further illustrated in Figures 6(d)–(f). Although affected by the noise, the tracking errors exhibit continuous fluctuations but converge within ranges of $[-0.14, 0.13]$, $[-0.205, 0.39]$, and $[-0.53, 0.67]$. The identification errors are shown in Figures 6(g)–(i), where parts of the noise interferences are compensated by the RISE feedback module, and $\tilde{\upsilon}_i$ fluctuates within a range of less than 0.05. This demonstrates that although the proposed algorithm is based on Assumption 1, it can effectively handle random noise beyond the assumption range, and the robustness of the controller is relatively high. The accuracy of the identification model is improved by the composite framework of the RISE structure and fuzzy learning. However, as evidenced by the weight curve in Figure 7, owing to interference from random noise, the weights of the identification model fail to converge to their optimal values, which is one reason for the decrease in the tracking accuracy of the system state. Figure 8 displays the response of the control input and the interference of white noise, where the oscillation frequency of the input is similar to that of the noise. Initially, within the first 0.5 s, the control input approaches ± 100 but subsequently decreases to no more than ± 28, attributed to the significant error in the identification model in the initial period.

5.2 Simulation of aircraft attitude system

Case 5: Attitude dynamics model of aircraft. The model of the attitude dynamics of the aircraft is represented as

$$\begin{cases} \dot{\boldsymbol{\sigma}} = \boldsymbol{R}\boldsymbol{\omega}, \\ \boldsymbol{J}\dot{\boldsymbol{\omega}} = -\dot{\boldsymbol{J}}\boldsymbol{\omega} - \boldsymbol{\Omega}\boldsymbol{J}\boldsymbol{\omega} + \boldsymbol{M}_0 + \boldsymbol{M}_\delta \boldsymbol{\delta} + \boldsymbol{d}, \end{cases} \tag{53}$$

where $\boldsymbol{\sigma} = [\phi, \theta, \psi]^{\mathrm{T}}$ is the attitude angle with the roll angle, pitch angle, and yaw angle. $\boldsymbol{\omega} = [p, q, r]^{\mathrm{T}}$ is the attitude angular velocity of the three channels (roll, pitch, and yaw). $\boldsymbol{R}$ is the coordinate transformation matrix. $\boldsymbol{J}$ is the moment-of-inertia matrix consisting of the nominal $\boldsymbol{J}_0$ and the perturbation $\Delta\boldsymbol{J}$. $\boldsymbol{M}_0$ is the unknown pitch moment, $\boldsymbol{M}_\delta$ is the pitch moment coefficient, $\boldsymbol{\delta} = [\delta_a, \delta_e, \delta_r]^{\mathrm{T}}$ is the pneumatic rudder with aileron, elevator, and rudder, and $\boldsymbol{d}$ is the external disturbance, including the time-varying moment of inertia $\boldsymbol{J}_t(t)$ and turbulent wind.

The controller parameters are set as $k_\sigma = 5\boldsymbol{I}$, $k_\omega = 8\boldsymbol{I}$, $\alpha_\sigma = 3\boldsymbol{I}$, $\alpha_\omega = 3\boldsymbol{I}$, $\gamma_\sigma = 100\boldsymbol{I}$, $\gamma_\omega = 100\boldsymbol{I}$, $\beta_\sigma = 10\boldsymbol{I}$, $\beta_\omega = 10\boldsymbol{I}$, $\Gamma_\sigma = 10\boldsymbol{I}$, $\Gamma_\omega = 10\boldsymbol{I}$, $c_1 = 1.2$, $c_2 = 0.5$, $a_\sigma = 5\boldsymbol{I}$, $a_\omega = 5\boldsymbol{I}$, $b_\sigma = 2\boldsymbol{I}$, $b_\omega = 2\boldsymbol{I}$, $k_{\sigma 1} = 0.1\boldsymbol{I}$, $k_{\omega 1} = 0.1\boldsymbol{I}$, $k_{\sigma 2} = 0.3\boldsymbol{I}$, $k_{\omega 2} = 0.3\boldsymbol{I}$, $m_{\sigma 1} = 0.05\boldsymbol{I}$, $m_{\omega 1} = 0.05\boldsymbol{I}$, $m_{\sigma 2} = 0.05\boldsymbol{I}$, and $m_{\omega 2} = 0.05\boldsymbol{I}$.

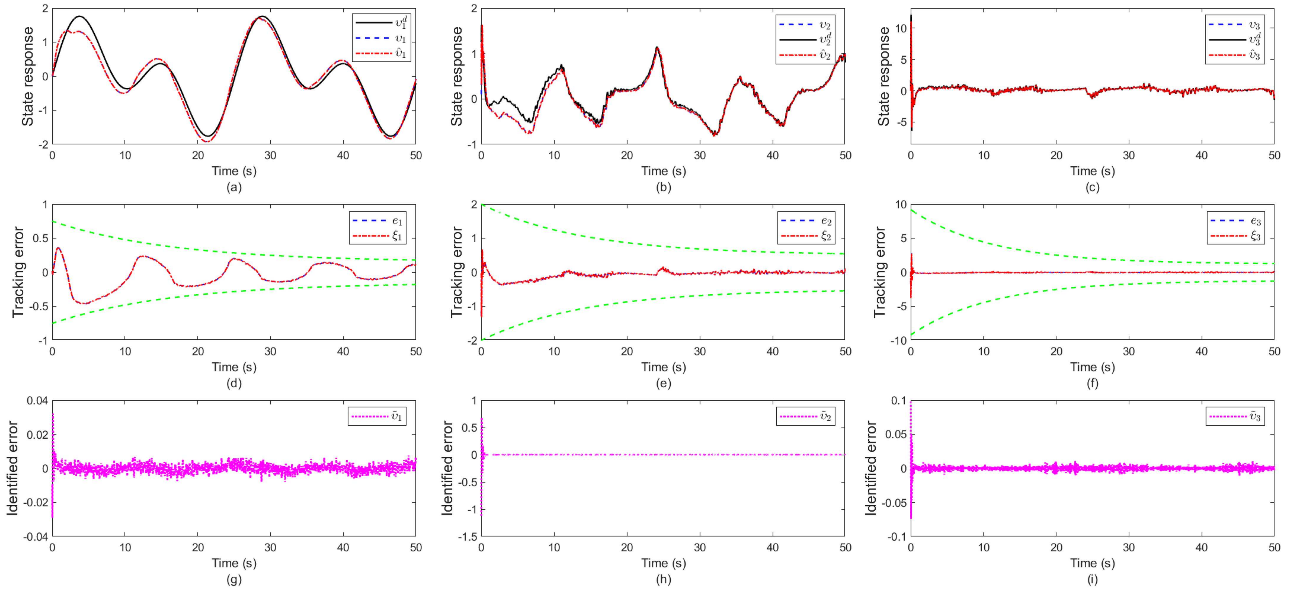

Figure 6 (Color online) System status tracking response and identification effect for Case 4. Tracking responses of (a) υ_1, (b) υ_2, and (c) υ_3; tracking errors (d) e_1 and ξ_1, (e) e_2 and ξ_2, and (f) e_3 and ξ_3; identification errors (g) $\tilde{\upsilon}_1$, (h) $\tilde{\upsilon}_2$, and (i) $\tilde{\upsilon}_3$.

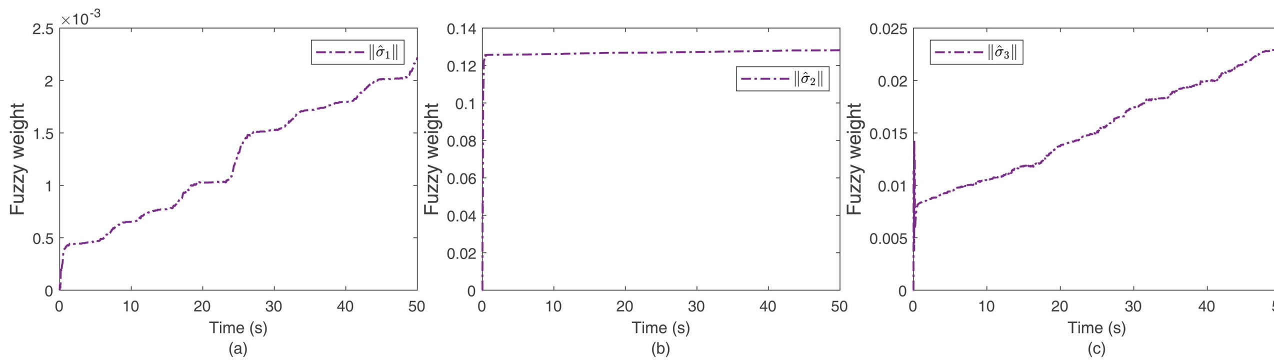

Figure 7 (Color online) Norm of fuzzy weight $\hat{\sigma}_i$ for Case 4. (a) $\|\hat{\sigma}_1\|$; (b) $\|\hat{\sigma}_2\|$; (c) $\|\hat{\sigma}_3\|$.

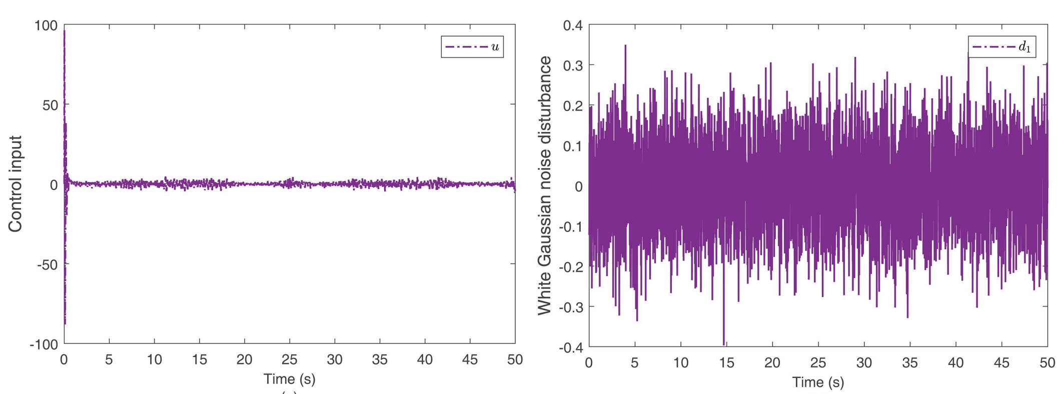

Figure 8 (Color online) (a) Control input u and (b) external disturbance d_1 for Case 4.

The simulation results obtained with the attitude system are shown in Figure 9. The roll angle ϕ, pitch angle θ, and yaw angle ψ all track the expected command signal. Moreover, the estimated response of the attitude angle of the system is consistent with that of the actual system. The tracking errors e_ϕ, e_θ, and e_ψ converge to a small neighborhood within 3.67 s. The estimated errors $\tilde{\phi}$, $\tilde{\theta}$, $\tilde{\psi}$ are almost zero after 6.5 s.

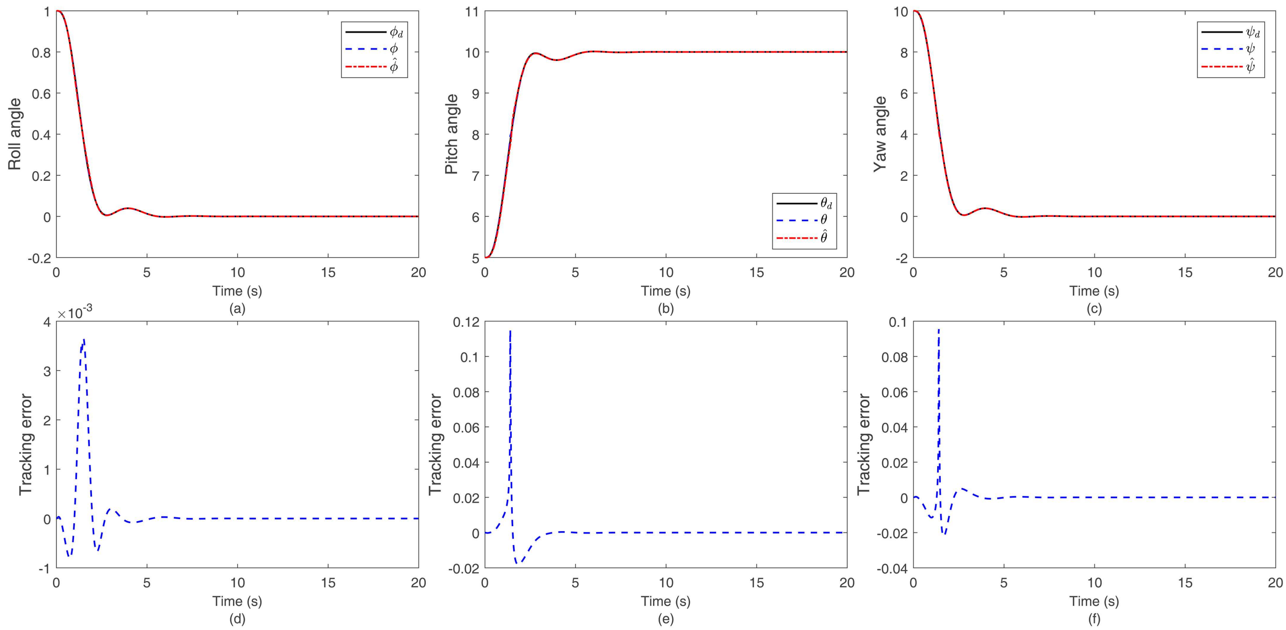

Figure 9 (Color online) Attitude angle tracking responses for Case 5. Tracking responses of (a) ϕ, (b) θ, and (c) ψ; tracking errors (d) e_ϕ, (e) e_θ, and (f) e_ψ.

6 Conclusion

This study addresses the impact of dynamic uncertainties and external disturbances on the stability of nonlinear system control by designing a state-estimation-based, prescribed fixed-time control algorithm. Two intelligent and robust techniques, FLS and RISE, are employed to establish a serial-parallel identification model. Using the identified dynamics, a control law is designed to ensure that the system states converge within a fixed time and remain within the preset performance constraints. The Lyapunov stability theorem is utilized to analyze the semi-global stability of the identification system and the fixed-time convergence of the control system. The proposed control method is applied to a third-order nonlinear system and the attitude system of an aircraft. The simulation results demonstrate that the identification accuracy is less than 0.001 and the state variables for the flight converge to near-zero within 6.5 s. The composite control method effectively handles bounded disturbances and reduces the impact of random noise on the control system to a certain extent.

In future work, practical engineering scenarios involving actuator and sensor faults will be thoroughly considered by incorporating fault-tolerant control strategies or extended-state observers. Additionally, because the proposed controller involves multiple key design parameters, techniques such as deep reinforcement learning will be explored for achieving automated and efficient parameter optimization.

Acknowledgements This work was supported by National Natural Science Foundation of China (Grant No. 62403131) and Jiangsu Funding Program for Excellent Postdoctoral Talent (Grant No. 2024ZB267).

References

1 Zhu J H, Yang Y J, Wang X Y, et al. Attitude control of a novel tilt-wing UAV in hovering flight. Sci China Inf Sci, 2023, 66: 154201
2 Su H Y, Lai J G. Distributed robust iterative learning control for AC microgrids with external disturbances. Sci China Inf Sci, 2025, 68: 202201
3 Lv C W, Ouyang Z Y, Wu Z H, et al. Practical tracking of MIMO uncertain stochastic systems driven by colored noises via active disturbance rejection control. Sci China Inf Sci, 2022, 65: 162208
4 Wang Z, Guo Z, Li S. Finite-time disturbance rejection control for rigid spacecraft attitude set stabilization with actuator saturation. IEEE Trans Aerosp Electron Syst, 2024, 60: 4910–4922
5 Niu B, Liu X, Guo Z, et al. Adaptive intelligent control-based consensus tracking for a class of switched nonstrict feedback nonlinear multiagent systems with unmodeled dynamics. IEEE Trans Artif Intell, 2023, 5: 1624–1634
6 Lu C X, Meng D Y, Li H Y. Data-induced learning control for unknown nonlinear systems with full-tracking performances. Sci China Inf Sci, 2025, 68: 182201
7 Xie H-X, Zhang J-X, Chai T Y. Adaptive tracking control of uncertain strict-feedback systems with tight self-adjustable performance guarantees. Sci China Inf Sci, 2025, 68: 192207
8 Wang C, Wang Z, Li W, et al. Composite disturbance filtering and full actuation control for fully observed systems. Sci China Inf Sci, 2025, 68: 172202
9 Chen M, Shi P, Lim C C. Robust constrained control for MIMO nonlinear systems based on disturbance observer. IEEE Trans Automat Contr, 2015, 60: 3281–3286
10 Jiang W, Ge S S, Li D. Fixed-time-synchronized control: a system-dimension-categorized approach. Sci China Inf Sci, 2023, 66: 172203

11 Ning P J, Hua C C, Li K, et al. A novel theorem for prescribed-time control of nonlinear uncertain time-delay systems. Automatica, 2023, 152: 111009
12 Zhou B, Ding Y, Zhang K-K, et al. Prescribed time control based on the periodic delayed sliding mode surface without singularities. Sci China Inf Sci, 2024, 67: 172204
13 Qu Z, Xu J. Model-based learning controls and their comparisons using Lyapunov direct method. Asian J Control, 2002, 4: 99–110
14 Xian B, Dawson D M, deQueiroz M S, et al. A continuous asymptotic tracking control strategy for uncertain nonlinear systems. IEEE Trans Automat Contr, 2004, 49: 1206
15 Wen H, Yue X, Wang Z, et al. Adaptive RISE control for asymptotic rigid-body attitude tracking with additive disturbances. ISA Trans, 2021, 117: 54–69
16 Zhao B, Zhang S, Liu D. Self-triggered approximate optimal neuro-control for nonlinear systems through adaptive dynamic programming. IEEE Trans Neural Netw Learn Syst, 2024, 36: 4713–4723
17 Zeng Y, Zhang F K, Chen T R, et al. Deterministic learning-based neural output-feedback control for a class of nonlinear sampled-data systems. Sci China Inf Sci, 2024, 67: 192202
18 Zhang J, Li S, Xiang Z. Adaptive fuzzy output feedback event-triggered control for a class of switched nonlinear systems with sensor failures. IEEE Trans Circuits Syst I, 2020, 67: 5336–5346
19 Deshmukh R R, Ballal M S, Suryawanshi H M. A fuzzy logic based supervisory control for power management in multibus DC microgrid. IEEE Trans Ind Applicat, 2020, 56: 6174–6185
20 Bounemeur A, Chemachema M. Finite-time output-feedback fault tolerant adaptive fuzzy control framework for a class of MIMO saturated nonlinear systems. Int J Syst Sci, 2025, 56: 733–752
21 Xu D, Jiang M, Hu W, et al. An online prediction approach based on incremental support vector machine for dynamic multiobjective optimization. IEEE Trans Evol Computat, 2021, 26: 690–703
22 Hamoudi Y, Abdolrasol M G, Amimeur H, et al. Open phase fault-tolerant support vector machine predictive power control for six-phase induction generator WECs. Energ Explor Exploit, 2025, 43: 744–775
23 Xu S, Liu J, Yang C, et al. A learning-based stable servo control strategy using broad learning system applied for microrobotic control. IEEE Trans Cybern, 2021, 52: 13727–13737
24 Chowdhury M, Keshmiri S. Interchangeable reinforcement-learning flight controller for fixed-wing UASs. IEEE Trans Aerosp Electron Syst, 2024, 60: 2305–2318
25 Liu C, Sun S S, Tao C G, et al. Optimizing evasive maneuvering of planes using a flight quality driven model. Sci China Inf Sci, 2024, 67: 132206
26 Liu Y J, Tong S. Adaptive fuzzy identification and control for a class of nonlinear pure-feedback MIMO systems with unknown dead zones. IEEE Trans Fuzzy Syst, 2014, 23: 1387–1398
27 Cherrat N, Boubertakh H, Arioui H. Adaptive fuzzy PID control for a class of uncertain MIMO nonlinear systems with dead-zone inputs nonlinearities. Iran J Sci Technol Trans Electr Eng, 2018, 42: 21–39
28 Ruan Z, Yang Q, Ge S S, et al. Adaptive fuzzy fault tolerant control of uncertain MIMO nonlinear systems with output constraints and unknown control directions. IEEE Trans Fuzzy Syst, 2021, 30: 1224–1238
29 Bounemeur A, Chemachema M, Essounbouli N. Indirect adaptive fuzzy fault-tolerant tracking control for MIMO nonlinear systems with actuator and sensor failures. ISA Trans, 2018, 79: 45–61
30 Bounemeur A, chemachema M, Zahaf A, et al. Adaptive fuzzy fault-tolerant control using Nussbaum gain for a class of SISO nonlinear systems with unknown directions. In: Proceedings of the 4th International Conference on Electrical Engineering and Control Applications: ICEECA 2019, Constantine, 2021. 493-510
31 Bounemeur A, Chemachema M. Adaptive fuzzy fault-tolerant control using Nussbaum-type function with state-dependent actuator failures. Neural Comput Applic, 2021, 33: 191–208
32 Patre P M, Bhasin S, Wilcox Z D, et al. Composite adaptation for neural network-based controllers. IEEE Trans Automat Contr, 2010, 55: 944–950
33 Wang X, Yu M, Yang L, et al. Airflow angles estimation-based finite-time adaptive neural control for aircraft at high-angle-of-attack maneuvers. IEEE Trans Syst Man Cybern Syst, 2025, 55: 5126–5136
34 Shou Y, Zhan T, Xu B, et al. Finite-time adaptive control of flexible hypersonic flight vehicle under measurement noise. IEEE Trans Aerosp Electron Syst, 2025, 61: 5826–5838
35 Kim D, Chung H, Bhasin S, et al. Robust composite adaptive fuzzy identification and control for a class of MIMO nonlinear systems. In: Proceedings of American Control Conference, 2011. 4947–4952
36 Liang S, Xu B, Sun S, et al. Dynamic-command-limiting-based AOA constraint control of hypersonic flight vehicle. IEEE Trans Aerosp Electron Syst, 2025, 61: 1163–1174
37 Wang L. Adaptive Fuzzy Systems and Control: Design and Stability Analysis. Englewood Cliffs: Prentice Hall, 1994
38 Lewis F L, Campos J, Selmic R. Neuro-Fuzzy Control of Industrial Systems with Actuator Nonlinearities. Philadelphia: SIAM, 2002
39 Patre P M, MacKunis W, Makkar C, et al. Asymptotic tracking for systems with structured and unstructured uncertainties. In: Proceedings of the 45th IEEE Conference on Decision and Control, 2006. 441–446
40 Bhasin S, Kamalapurkar R, Dinh H T, et al. Robust identification-based state derivative estimation for nonlinear systems. IEEE Trans Automat Contr, 2012, 58: 187–192
41 Sun Z Y, Yun M M, Li T. A new approach to fast global finite-time stabilization of high-order nonlinear system. Automatica, 2017, 81: 455–463
42 Sun Z Y, Shao Y, Chen C C. Fast finite-time stability and its application in adaptive control of high-order nonlinear system. Automatica, 2019, 106: 339–348
43 Xu B, Shou Y, Wang X, et al. Finite-time composite learning control of strict-feedback nonlinear system using historical stack. IEEE Trans Cybern, 2023, 53: 5777–5787
44 Levant A. Higher-order sliding modes, differentiation and output-feedback control. Int J Control, 2003, 76: 924–941
45 Sun J, He H, Yi J, et al. Finite-time command-filtered composite adaptive neural control of uncertain nonlinear systems. IEEE Trans Cybern, 2020, 52: 6809–6821
46 Wang F, Xie X, Lv Z, et al. Adaptive neural network fixed-time fault-tolerant control of an uncertain nonlinear system with full-state constraints. Inf Sci, 2022, 608: 858–880
47 Wang Z, Hu C, Zhu Y, et al. Neural network learning adaptive robust control of an industrial linear motor-driven stage with disturbance rejection ability. IEEE Trans Ind Inf, 2023, 13: 2172–2183
48 Chen M, Ma H, Kang Y, et al. Adaptive neural safe tracking control design for a class of uncertain nonlinear systems with output constraints and disturbances. IEEE Trans Cybern, 2022, 52: 12571–12582